Uniwersytet Warszawski

Wydział Fizyki

Beata Pawlukiewicz - Kamińska
Nr albumu: 196065

Simulation of the *Bremsstrahlung* Emission by Hadrons in the COMPASS Experiment

Praca magisterska
na kierunku Fizyka
w zakresie Fizyki Cząstek i Oddziaływań Fundamentalnych

Praca wykonana pod kierunkiem
prof. Barbary Badełek
Uniwersytet Warszawski

WARSZAWA, lipiec 2005

Oświadczenie kierującego pracą

Oświadczam, że niniejsza praca została przygotowana pod moim kierunkiem i stwierdzam, że spełnia ona warunki do przedstawienia jej w postępowaniu o nadanie tytułu zawodowego.

Data Podpis kierującego pracą

Oświadczenie autora pracy

Świadoma odpowiedzialności prawnej oświadczam, że niniejsza praca dyplomowa została napisana przeze mnie samodzielnie i nie zawiera treści uzyskanych w sposób niezgodny z obowiązującymi przepisami.

Oświadczam również, że przedstawiona praca nie była wcześniej przedmiotem procedur związanych z uzyskaniem tytułu w wyższej uczelni

Oświadczam ponadto, że niniejsza wersja pracy jest identyczna z załączoną wersja elektroniczną.

Data Podpis autora (autorów) pracy

Streszczenie

Celem niniejszej pracy jest próba oszacowania wielkości elektromagnetycznych poprawek radiacyjnych w wierzchołku hadronowym dla nieelastycznego rozpraszania $\mu^+ N$ w eksperymencie COMPASS. Symulacje poprawek radiacyjnych zostały wykonane programem Monte Carlo PHOTOS. Analizie poddane zostały pędy pionów pochodzących z rozpadu ρ^0, pędy par hadronów o wysokim pędzie poprzecznym w obszarze $Q^2 < 1$ GeV^2 oraz inwariantna masa inkluzywnie produkowanego ρ^0. Uwzględnienie efektów radiacyjnych w rozpadach hadronów daje zmiany w analizowanych rozkładach nie przekraczające 2%.

Słowa kluczowe

spinowa struktura nukleonu, polaryzacja gluonów, poprawki radiacyjne QED, rozpady hadronów, symulacja Monte Carlo, PHOTOS, PYTHIA

Dziedzina

13.2 fizyka

Dedykuję Mężowi i naszemu Dziecku.

Contents

List of Figures

List of Tables

Chapter 1

Introduction

1.1 The Spin Puzzle

Spin is one of the fundamental properties of elementary particles. Spin quantum number of the nucleon is 1/2. It can be decomposed into the contributions from its constituents:

$$\frac{1}{2} = \frac{1}{2}\Delta\Sigma + \Delta G + L. \tag{1.1}$$

Here $\Delta\Sigma$ is a contribution from the spin of quarks[1] and is a difference of the number of quarks with the spin parallel and antiparallel to the spin of the nucleon, ΔG is a contribution from the spin of gluons and L stands for a contribution from quarks' and gluons' orbital momentum. In the naive *Quark Parton Model* (QPM), which provides a description of several properties of hadrons, e.g. charges and magnetic moments, the nucleon spin is determined by the spin of three S-state valence quarks: two quarks having spins parallel to the spin of the nucleon, the third – antiparallel. In this model $\Delta\Sigma = 1$ and all the other contributions are equal to 0, while assuming QPM, SU(3) and a null polarisation of strange quarks, gives $\Delta\Sigma \approx 0.6$ and $\Delta G = L = 0$. In this context the result of the EMC experiment in 1988 came as a surprise: they found that $\Delta\Sigma = 0.14 \pm 0.09$ $(stat) \pm 0.21$ (sys)[2] [1] which means that only a small part of the nucleon spin originates from the spin of quarks. The SMC experiment CERN, designed to cross-check and improve the EMC results, confirmed them: $\Delta\Sigma = 0.19 \pm 0.05$ $(stat) \pm 0.04$ (sys)[3] [2].

A probable conclusion from the EMC and SMC results is that the gluon contribution to the spin of the nucleon is nonzero. ΔG value may in principle be extracted from the next-to-leading-order chromodynamic evolution of the structure function g_1. However, because of the poor quality of the g_1 data, ΔG is determined with approximately 100% error [2]. Therefore, direct measurements of ΔG are highly desirable.

[1] The term "quarks" encompasses both quarks and antiquarks.

[2] Assuming that the contribution of strange quarks polarisation to the nucleon spin is zero.

[3] The $\Delta\Sigma$ value is given at $Q^2 = 1$ GeV^2 and in the $\overline{MS}$ scheme.

1.2 Experiments Dedicated to Spin Physics

New experiments, with a wide spin physics programme contributing to solve the spin puzzle, have been designed and are presently running: HERMES at DESY, COMPASS at CERN, STAR and PHENIX at BNL and several experiments at JLAB.

The most important goals of the spin physics programme in the HERMES experiment are measurements of the flavour decomposition of the quarks polarisation in the nucleon, the structure functions of proton, deuteron and neutron, the gluon polarisation in the nucleon and the transversity. Experiments at JLAB are focused on investigating the nucleon spin structure functions in the resonance region and at low Q^2 and on testing the generalised Gerasimov-Drell-Hearn sum rule. HERMES and the experiments at JLAB use polarised electron beams with the incident energy of 27.5 GeV and in the range $1 - 6$ GeV, respectively. HERMES uses polarised gases (H, D, ${}^3He$) injected into the internal cell target in the storage ring; polarisation of the target material is frequently inverted. Highly intensive electron beams and small sizes of the targets which are used in these experiments make them not too sensitive to systematic effects caused by changes in the detector acceptance. Kinematic ranges of these experiments are limited because of relatively low incident energies.

Experiments STAR and PHENIX at RHIC, dedicated to collide heavy ions, are the first experiments in the world that collide also the polarised proton beams. They will be polarised up to 70% with the centre-of-mass energy up to 500 GeV. These experiments will cover a large kinematic range of x_g, which is a fraction of the nucleon momentum carried by a gluon, from 0.01 up to 0.3. The colliding protons are probing each other and ΔG is measured through the cross-section asymmetries in the production of $pp \to \gamma + jet + X$ or $pp \to jet + jet + X$ events. The quark flavour contributions to the proton spin and the transversity belong to the main aims of the spin physics of the STAR and PHENIX experiments.

1.3 COMPASS

COMPASS (COmmon Muon and Proton Apparatus for Structure and Spectroscopy) is a high energy physics experiment dedicated to study the hadron structure and spectroscopy. It is a fixed target experiment with muon and hadron beams. Main goals in its muon programme are to investigate the gluon contribution to the spin of the nucleon (for $0.07 < x_g < 0.15$), spin dependent parton distributions, the transversity, Λ polarisation and the exclusive production of vector mesons. Physics data taking began in 2002.

COMPASS investigates inelastic $\mu^+ N$ scattering processes where N stands for the nucleon.

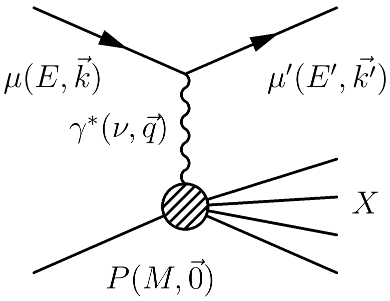

Figure 1.1: Feynman diagram of a DIS process. In parentheses energies and momenta in the LAB frame are given.

A Feynman diagram for this reaction in the one photon exchange[4] (Born) approximation is shown in Fig. 1.1. The kinematic variables are defined in the laboratory frame (LAB) as follows:

$$Q^2 = -q^2 \approx 2EE'(\cos\theta - 1), \quad \nu = E - E', \quad x = \frac{Q^2}{2M\nu}, \quad y = \frac{\nu}{E}. \tag{1.2}$$

Here E and E' are the energies of the incoming and scattered muon, respectively, θ is the muon scattering angle, ν stands for the virtual photon energy, M – for the nucleon mass, Q^2 is the virtuality of the exchanged photon, x has the interpretation of a fraction of the nucleon momentum carried by a struck parton in the *infinite proton momentum frame* and finally y is a fraction of the muon energy transferred to the virtual photon. At a given energy the cross section for the inelastic μ^+N scattering is described by two variables, usually Q^2 and x or y.

The gluon polarisation ΔG is measured from the spin dependent cross sections asymmetries of the photon-gluon fusion process (PGF), cf. Fig. 1.2, which are directly proportional to ΔG. PGF is a process in which a (polarised) virtual or quasi-real photon coming from a (polarised) muon beam interacts with a (polarised) gluon from the nucleon via a $q\overline{q}$ pair. Photons which do not have electromagnetic charge cannot couple to gluons directly. In particular, a creation of a $c\overline{c}$ pair (PGF$_{c\overline{c}}$) or of a light $q\overline{q}$ pair (PGF$_{q\overline{q}}$) with high transverse momenta p_T[5] is a good signature that the γ^*N interaction indeed took place through the PGF process. A large mass of the charm quarks, about $1 - 1.4$ GeV [3], or high p_T value of light quarks ($\gtrsim 0.7$ GeV) set the QCD energy scale appropriate for perturbative calculations independently of the Q^2 value[6].

The PGF$_{c\overline{c}}$ process has a very low background as the probability of $c\overline{c}$ creation in the

[4] Exchange of the Z^0 boson is negligible at the COMPASS centre-of-mass energy (about 18 GeV).
[5] p_T is defined with respect to the γ^* momentum.
[6] The energy scale in DIS processes is usually defined by $Q^2 \gtrsim 1\text{GeV}^2$.

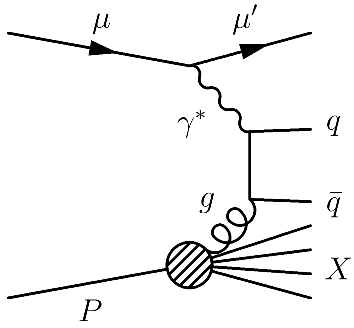

Figure 1.2: The photon-gluon fusion diagram.

hadronisation process or in the γ^* interaction with a charm sea quark is negligible. On the contrary, the $\mathrm{PGF}_{q\overline{q}}$ process has a large background of other photon interactions with a nucleon, e.g. QCD Compton scattering, $\gamma^* q \rightarrow q$, or photoabsorption, $\gamma^* q \rightarrow g + q$. The $c\overline{c}$ pair fragments then into charm mesons like D^0 or D^* and the light $q\overline{q}$ pair into any hadron characterised by high p_T. In COMPASS D^0 and D^* are identified through their hadronic decays: $D^{*\pm} \rightarrow D^0\pi^{\pm} \rightarrow K^+\pi^-\pi^{\pm}$. Therefore a correct identification of hadrons and a correct measurement of their four-momenta is crucial for the data analysis.

Chapter 2

The COMPASS Experiment

Direct measurements of ΔG require a fragmentation of a $c\overline{c}$ pair into D^0 or D^* mesons or a fragmentation of a light $q\overline{q}$ pair into hadrons with high p_T. In the final state we need to identify the D meson decay products and to measure their four-momenta. The incident and outgoing muons have to be detected as well. In this Chapter a brief description of the COMPASS experimental setup and of some aspects of the data analysis is presented.

2.1 The Beam

The COMPASS experiment is situated at the CERN SPS M2 muon beam line. Every 16.2 seconds a 400 GeV proton beam from the Super Proton Synchrotron (SPS) interacts with a beryllium target resulting in a beam of secondary particles: $K^{\pm}$, $\pi^{\pm}$, p^+ of which positive pions are selected. During 400 m long way they decay into muons and muon neutrinos as in the example reaction: $\pi^+ \rightarrow \mu^+ \, \nu_\mu$. Other hadrons are absorbed in an absorber wall whereas muons come through it loosing only small part of their initial energy. At last a set of magnets situated on a 600 m long way forms the muon beam. It is longitudinally polarised through the π decay mechanism. The 76% polarisation at the 160 GeV energy with 3% spread result from a compromise between these two parameters in the laboratory frame[1]. The beam intensity is $2.8 \cdot 10^8$ μ^+ per 4.8 seconds long SPS spill.

2.2 The Target

A muon scattering on a deuteron is presently investigated in COMPASS. A target filled with solid lithium deuteride ^6LiD is used to achieve this aim. Assuming that the weakly bound ^6Li nucleus consists of an alpha particle and of a deuteron, the nominal dilution factor of ^6LiD is equal to 0.5. The target material is, however, not pure and contains a few percent contamination of other elements like He, ^7Li, H, F, Cu and thus the dilution factor decreases to about 0.4. Polarisable part of the target material reaches a polarisation

[1]Transformation to the LAB makes the polarisation inversely proportional to the muon energy.

of about 57% obtained through the *Dynamic Nuclear Polarisation* method. The target consists of two cells. Each cell is 60 cm long and 3 cm in diameter. Cells are placed parallel one after another with 10 cm gap between. They are placed in the 2.5 T solenoid field and cooled down to the temperature of 50 mK. To reduce systematic errors the cells are polarised in opposite directions, longitudinally (transversally) with respect to the beam momentum; their polarisation is reversed every 8 hours.

2.3 The Spectrometer

The spectrometer, Fig. 2.1, consists of magnets, tracking detectors, calorimeters and particle identification devices grouped into two stages. Large Angle Spectrometer (LAS) is designed to detect fast particles with emission angles up to 180 mrad and Small Angle Spectrometer (SAS) – to detect slow particles with emission angles up to 30 mrad.

Particle momenta measurements are performed using two magnets: SM1 and SM2. Particle identification is accomplished by the Ring Imaging Cherenkov counter, RICH (up to now only in LAS), hadron calorimeters in both stages, Hadron-Calorimeter 1 and 2, electromagnetic calorimeters, EM-Calorimeter (in LAS only) and muon detectors, Muon-Filter1 and Muon-Filter2. RICH is designed to separate pions and kaons with momenta greater than 3 GeV and 10 GeV, respectively. Information about particle tracks in the region close to the beam is provided by the GEMs and MicroMegas detectors, by stations of scintillating fibers and by silicon detectors. Tracking in the outer region is provided by drift and straw trackers placed upstream and downstream the two magnets.

Interesting events are selected by the trigger system. The triggers select an event if the incoming and outgoing muon in a proper time correlation were recorded. Almost all physics triggers additionally require a signal from the hadron calorimeters. The last condition means that only inelastic $\mu^+ N$ events are recorded, *i.e.* events where X in Fig 1.1 is different from a nucleon.

2.4 Data Flow and Acceptance

COMPASS collects daily about 3 TBytes of data. During 2002 – 2004 about 950 TBytes of data were collected. The $2002 + 2003$ sample contained about 1500 events of D^*, about 28000 events with high p_T hadron pairs for $Q^2 > 1$ GeV^2 and about 250000 events with high p_T hadron pairs for $Q^2 < 1$ GeV^2. In 2004 a total amount of collected data was two times larger than in 2002 + 2003, therefore the number of interesting events should also double after including the 2004 sample[2]. The kinematic acceptance covered in the 2002

[2]Analysis of 2004 is not completed yet.

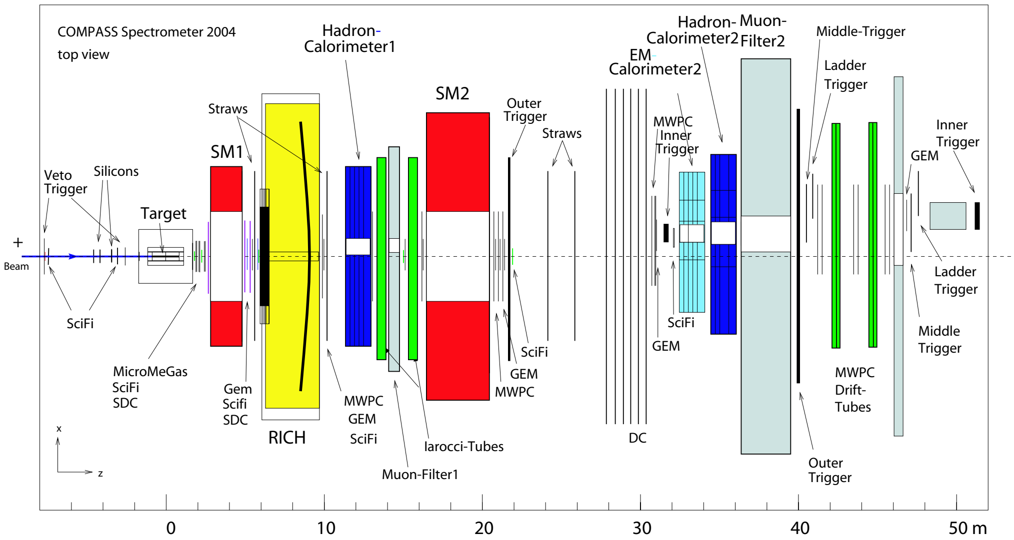

Figure 2.1: Top view of COMPASS lay-out in 2004.

run is shown in Fig. 2.2 and is approximately the same also for the remaining part of the data.

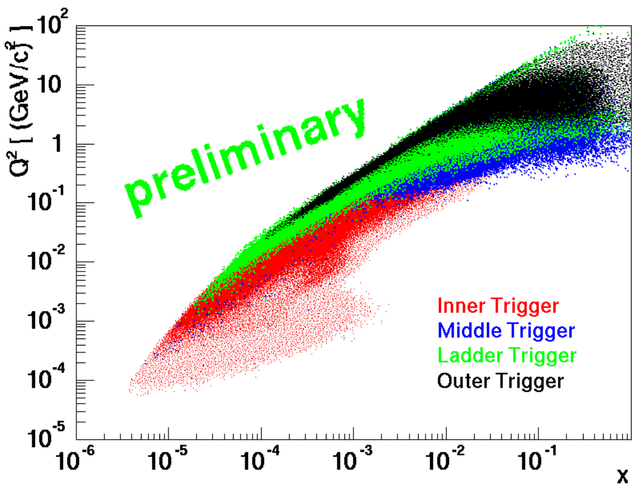

Figure 2.2: COMPASS kinematic acceptance in 2002.

This acceptance is characteristic for all the fixed target experiments, *i.e.* an arrow-like shape with a very strong correlation between low Q^2 and low x regions.

2.5 Radiative Processes

Experimentally measured $\mu^+ N$ cross sections are always affected by radiative effects. In Fig. 2.3 radiative processes contributing to DIS (diagram a, later denoted by $\sigma_{1\gamma}$) to order α^3, where $\alpha = e^2/4\pi\epsilon_o\hbar c \simeq 1/137$ is the electromagnetic fine-structure constant, are shown. Diagram b is a contribution from the vacuum polarisation, where in the loop a $q\overline{q}$ or $l\bar{l}$ pair can be created. Diagrams c and f show remaining virtual processes and diagrams d, e and g – a real photon emission (*bremsstrahlung*). Virtual processes are not experimentally observed; neither is *bremsstrahlung* emission in COMPASS due to the poor photon detection by its spectrometer. Therefore reactions b – g, which constitute a background to the Born cross section, $\sigma_{1\gamma}$, cannot be removed from the sample on an event-by-event basis. Contributions to $\sigma_{1\gamma}$ from these processes are called *internal radiative corrections*[3]. The largest contributions are given by reactions d and e, which additionally may occur in the elastic way but faking DIS. There are also *external radiative corrections* which result from the lepton *bremsstrahlung* on the target material. This type of the radiative corrections is negligible for muon beams. The aim of the data analysis is to extract the differential cross section in the one photon exchange approximation ($\sigma_{1\gamma}$) from the data (σ_{meas}).

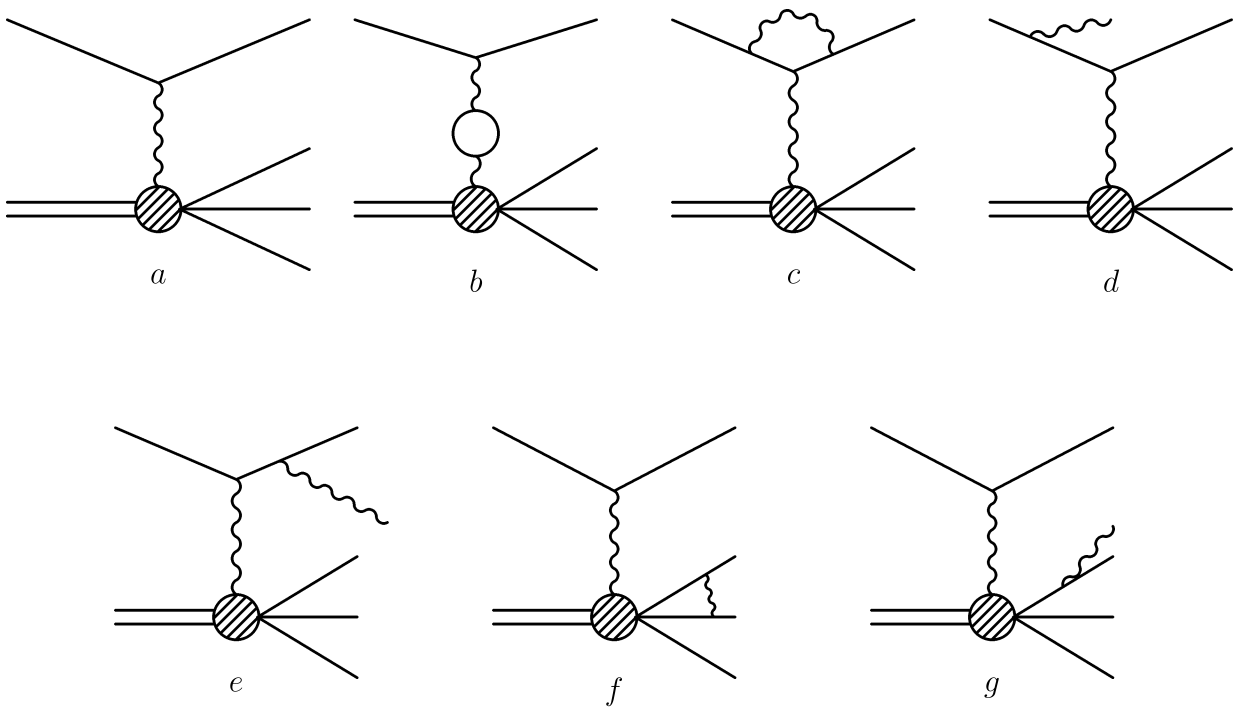

Figure 2.3: Radiative processes (b – g) contributing to the DIS cross section (a) at the order α^3.

[3]Later called also radiative corrections (RC).

In the analysis the radiative effects are corrected for (x, y) bins and the radiative correction factor, calculated theoretically, is defined as:

$$\eta(x,y) = \frac{\sigma_{1_\gamma}(x,y)}{\sigma_{meas}(x,y)}. \tag{2.1}$$

Spin data require the knowledge of radiative corrections for both spin averaged and spin dependent cross sections.

Virtual corrections affect the measured yields. Real photon emission affect both the yields and the reaction kinematic variables in this way that the true values of those variables are shifted towards smaller (Q^2, ν, y) or larger values (x). The largest and most significant are the corrections for small x and high y, e.g. for $x = 10^{-5}$ and $y = 0.95$, $\eta \simeq 100$ and a measured cross section is almost exclusively radiative. In the COMPASS a huge radiative contribution from the elastic part of diagrams d and e is suppressed by a trigger requirement of energy deposit in the hadron calorimeter. Therefore, radiative corrections in the COMPASS kinematic range are of the order of 10% ($\eta \simeq 1.1$).

There are two independent approaches to calculate RC in the lepton vertex (diagrams b, c, d and e in Fig. 2.3). The first one, proposed by L.W. Mo and Y.S. Tsai in the sixties (the MT scheme [5]), was written for the electron scattering experiments at SLAC. The second, conceived in the seventies, was created by the Dubna group (the D scheme [6]) for the muon scattering experiment BCDMS at CERN. A basic difference between these two approaches is that the D scheme, which is formulated in a covariant way, is independent of the infrared cut-off parameter Δ[4] and the MT scheme, formulated in a noncovariant way, contains explicit dependence on this parameter. A detailed comparison of those two approaches was done in 1994 [7] resulting in the conclusion that both schemes are in the agreement and the difference between them in the region of low x and high y is of the order of 2%. FERRAD, the first program calculating the radiative corrections, is based on the MT scheme. TERAD and POLRAD (the latter additionally takes into account the beam and target polarisations) are based on the D scheme. All these programs calculate QED corrections for the lepton vertex only. They need to be provided with the measured kinematic variables of the reaction, elastic and quasielastic form factors of the target, nucleon structure functions and some initial information, e.g. the incident energy. As a result they return the correction factor η and the cross section $\sigma_{1\gamma}$.

It was always assumed that the radiative corrections in the hadron vertex (diagrams f and g, Fig. 2.3) are small and negligible. This work is a first quantitative attempt to estimate the radiative effects in the hadron vertex for the COMPASS experiment and thus to estimate their influence on charged pions spectra. Hadron high p_T pairs are sensitive tools to probe ΔG in the nucleon [4] and therefore every possible systematic bias of them has to be carefully checked.

[4] Δ may be attributed a meaning of the energy resolution, *i.e.* maximal energy of photons not recorded in the experiment.

Chapter 3

Monte Carlo in the Data Analysis

In this Chapter Monte Carlo programs used in the analysis of the COMPASS data are described. Particular attention is given to the PYTHIA generator.

3.1 Monte Carlo Programs in COMPASS

There are three Monte Carlo event generators widely used in the COMPASS analysis: PYTHIA [8], AROMA [9] and LEPTO [10]. These MC programs are all based on the Lund fragmentation model and are used in the simulation of the PGF processes: LEPTO in the region of high Q^2, PYTHIA in the region of low Q^2 and AROMA for events with charm mesons in the final state. The Monte Carlo output is then processed by COMGEANT and CORAL programs which simulate detector response and perform event reconstruction, respectively. This Monte Carlo chain: PYTHIA (AROMA or LEPTO) + COMGEANT + CORAL thus simulates the experimental data. A correct simulation of the detector behaviour is crucial. If a discrepancy between the Monte Carlo and real data is observed in spite of the correct detector simulation, one might suspect that the event generator does not describe the reality properly and that an appropriate MC tuning is necessary. There are over few hundred parameters in any MC program which control a generated process, e.g. such key issues as parton momentum distributions in the nucleon, fragmentation functions or a choice of an appropriate energy scale for a given process.

A simulation presented in this thesis was obtained by a modified PYTHIA generator only and thus is not a result of the full Monte Carlo chain: neither COMGEANT smearing nor the CORAL reconstruction was performed. Therefore all the results presented here should be treated as upper limits of analysed effects.

3.2 PYTHIA Generator

The PYTHIA generator is dedicated to simulate multiparticle production in collisions of elementary particles. COMPASS uses PYTHIA to simulate photon-gluon fusion processes with hadron production in the region of $Q^2 < 1\,\mathrm{GeV}^2$ and as a background for open charm mesons events.

All the simulations presented here are done using PYTHIA 6.205. The $\mu^+ N$ events are generated for the incident muon of energy 160 GeV and a fixed proton[1] target. All the PYTHIA parameters are left at their values default except the limits on Q^2: the lower limit for Q^2 is set: $Q^2_{min} = 10^{-6}\,\mathrm{GeV}^2$ and the upper: $Q^2_{max} = 1\,\mathrm{GeV}^2$. The default values of the remaining variables are: $x \in (0, 1)$, $y \in (0.0001, 0.99)$.

3.3 Properties of the Particles in the Final State

Inelastic $\mu^+ N$ scattering produces many hadrons in the final state. Simulating this process using PYTHIA we find in its event record so called stable particles. By them we mean both charged and neutral particles whose lifetime is grater then 10^{-8} s. Such particles before decaying can run a distance of several meters which is enough to be detected in a spectrometer. In a typical final state we find the following stable particles: μ^+, $\pi^\pm$, $K^\pm$, K^0_L, p, n, γ. Especially interesting are charged particles because the COMPASS spectrometer is well equipped to detect them[2]. On average there are about 12.3 stable particles produced in the final state of an event. Particle multiplicities are given in Table 3.1.

μ^+	$\pi^\pm$	$K^\pm$	K^0_L	p	n	γ
1.00	4.37	0.34	0.16	0.66	0.49	5.24

Table 3.1: Average particle multiplicities in the final state of a $\mu^+ p$ event.

Most of stable particles in the final state are $\pi^\pm$, then $K^\pm$. A scattered muon is always present. Charged pions, kaons and protons are used in the high p_T hadron analysis.

About 70% of pions and 50% of kaons result from decays. This information is crucial for further analysis with PHOTOS, a Monte Carlo program which simulates radiative corrections exclusively in particle decays. If pions and kaons would originate directly from

[1]Simulation on a proton target is a good approximation of a scattering on a deuteron target.

[2]The COMPASS detector records hadrons with energy $\gtrsim$ 0.5 GeV.

the hadronisation processes usage of PHOTOS would not make sense. In Tables 3.2 and 3.3 the origin of pions and kaons in the μ^+p event generated by Pythia is shown.

origin of $\pi^{\pm}$	percent of $\pi^{\pm}$ mesons originating in a decay
ρ^0	18.4%
$\rho^{\pm}$	16.8%
ω	15.7%
K_s^0	4.9%
η	3.7%
Δ^{++}	3.0%
$K^{*\pm}$	2.6%
λ^0	1.4%
$\eta^{'}$	1.2%
K^{*0}	1.2%

Table 3.2: Origin of pions normalised to the number of pions resulting from decays in a μ^+p event.

origin of $K^{\pm}$	percent of $K^{\pm}$ mesons originating in a decay
$K^{*\pm}$	17.1%
K^{*0}	15.1%
$\overline{K^{*0}}$	11.9%
ϕ	4.3%

Table 3.3: Origin of kaons normalised to the number of kaons resulting from decays in a μ^+p event.

Charged pions come mainly from the decays of resonances such as ρ^0, $\rho^{\pm}$, ω, η, Δ and from the decays of other particles like K^*, K_S^0, Λ^0. Charged kaons are mainly results of K^*, D^0 and ϕ decays. The largest number of pions come from the ρ^0 decays. Therefore in what follows we shall limit the analysis to the $\rho^0 \to \pi^+\pi^-$ decay channel.

Chapter 4

PHOTOS

In this chapter a brief description of Monte Carlo programs used to estimate the QED radiative corrections is given, then general properties of PHOTOS and its implementation are described.

4.1 RADGEN

RADGEN [11] is a Monte Carlo program generating radiative corrections in DIS processes. It was written by I. Akushevich, H. Böttcher and D. Ryckbosch for the HERMES experiment. RADGEN, based on the MT scheme, generates radiative corrections in the lepton vertex taking into account diagrams $b - f$ in Fig. 2.3. HERMES was first to combine RADGEN with the PYTHIA generator [12] to improve the background simulation; later also COMPASS used this tool. RADGEN as well as earlier described programs generating RC for the lepton vertex (TERAD, FERRAD, POLRAD) do not compute radiative effects from non point-like particles, *i.e.* hadrons.

4.2 PHOTOS

PHOTOS is a Monte Carlo program generating QED radiative corrections in the decays of particles. First version of PHOTOS was written by E. Barberio, B. van Eijk and Z. Wąs in 1991 [13]. The latest version, developed by P. Golonka and Z. Wąs, was completed at the end of February 2005. All the versions are available on the home page of Z. Wąs [14]. Analysis presented in this thesis is based on the latest available version of PHOTOS, PHOTOS 2.13, used with multiphoton emission option.

4.2.1 General properties of PHOTOS

PHOTOS generates QED radiative corrections in the approximation of collinear emission (leading logarithm) with a proper treatment of the infrared limit (cut-off). Non-collinear emission is also simulated, however validity of it may be restricted, see Sec. 5.3.3. Diagrams for single photon emission processes, which are taken into account by PHOTOS, are shown in Fig. 4.1. Higher order corrections in the leading-logarithmic approximation (emission of n photons) are obtained by an iterative procedure[1]. Diagrams with double photon emission are shown in Fig. 4.2. Approximations used in PHOTOS were tested and optimized for decays of vector bosons into fermions, e.g. $Z^0 \to f\overline{f}$. It was checked that they are correct with the exception of negligibly small parts of the photon phase space; they were analysed for Z and W decays [15]. PHOTOS was not optimized for decays of vector mesons into scalars, e.g. $\rho^0 \to \pi^+\pi^-$, which are mainly considered in this thesis. However, it is assumed that the obtained results are correct in the same range of the photon phase space as the results for the Z or W decays.

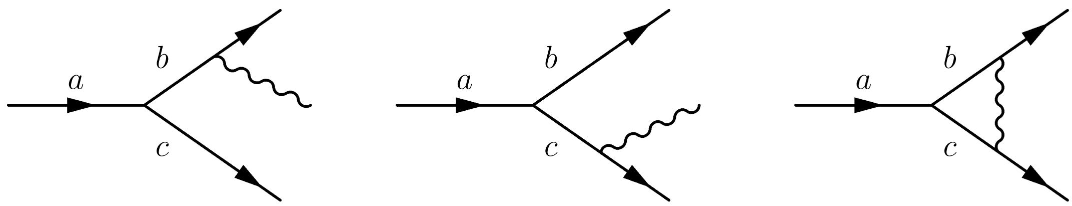

Figure 4.1: Radiative corrections generated by PHOTOS in the first iteration.

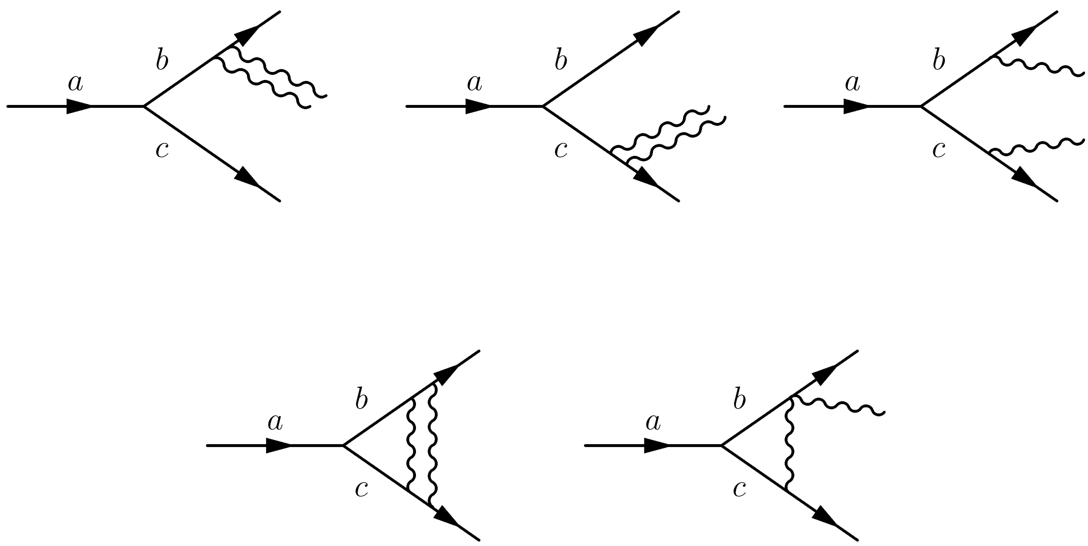

Figure 4.2: Radiative corrections generated by PHOTOS in the second iteration (in addition to those already presented in Fig 4.1).

[1]Iterative procedure means that if in a given decay with k particles in the final state one *bremsstrahlung* photon was emitted and all the kinematic variables were accordingly changed, the new final state of $k+1$ particles is treated as an initial configuration for the next photon generation.

4.2.2 PHOTOS and PYTHIA

PHOTOS works with the "standard output" of any Monte Carlo program and modifies it by adding *bremsstrahlung* photons. The output of a Monte Carlo program used together with PHOTOS has to be stored in a standard format. PHOTOS interfaces with the generator via the HEPEVT event record and works with the default PYTHIA mode of the HEPEVT common block filling (MSTP(128)=0). There are several problems with running PHOTOS on the PYTHIA output. A typical one is that the "mother-daughter" relations are incorrectly filled, e.g. particles labeled "stable" decay and become mothers of secondary particles. The event is thus not a consistent cascade decay. An algorithm correctly finding all the decays ("trees") in a event record, not universal but applicable for $\mu^+ N$ events generation, was constructed by B. Kersevan for the ATLAS experiment [16].

4.2.3 Implementation of PHOTOS

PHOTOS is called after event generation by PYTHIA for the highest mother of each decay tree and goes through all its decay branches. If there is at least one charged daughter in a branch a probability of the photon emission is calculated. If this probability is large enough, all photon characteristics are generated. Next, the four-momenta of both charged and neutral daughters as well as of the further particles in a cascade decay are changed accordingly. Finally the output is reordered and the generated photon is added as the last daughter of the decaying particle.

4.2.4 Test of the correct implementation of PHOTOS

A basic test of the correct PHOTOS implementation is a check of the energy conservation in the hadron vertex. A quantity ΔE was calculated for each PYTHIA generated event according to the equation:

$$\Delta E = E + M - \sum_i E_i \tag{4.1}$$

where E_i denotes energy of the particle i in the final state. Distributions of ΔE before and after PHOTOS implementation are shown in Figures 4.3– 4.4. As expected ΔE is indeed very close to zero in both cases; implementation of PHOTOS does not change the distribution width at all.

4.3 PHOTOS Parameter Tuning

One of the most important parameters in the QED radiative corrections calculations is a threshold for soft photon emission (infrared cut-off) Δ which is essential to obtain finite values of observables. All the observables should however be insensitive to the change of this parameter within reasonable limits. In PHOTOS the value of Δ may be controlled using XPHCUT parameter, which defines the minimum photon energy expressed as a

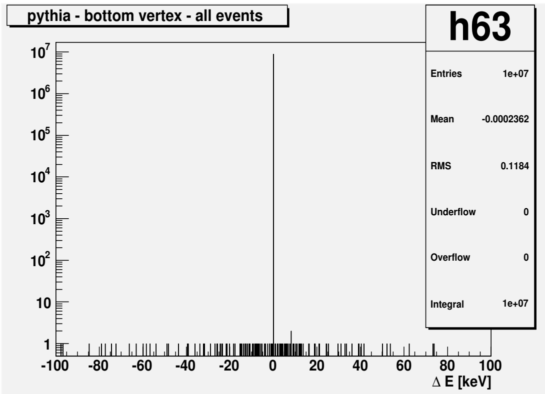

Figure 4.3: Energy conservation in the bottom vertex for the events generated by PYTHIA.

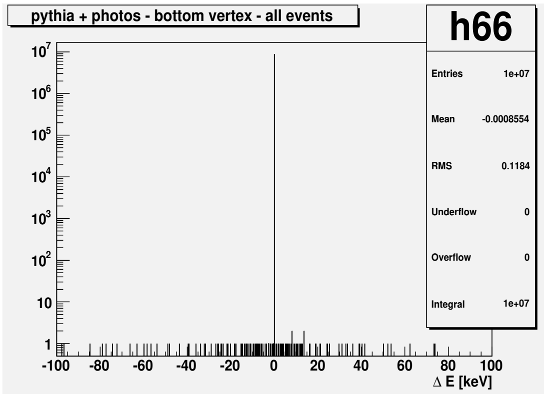

Figure 4.4: Energy conservation in the bottom vertex after PHOTOS implementation to PYTHIA.

fraction of decaying particle mass. The XPHCUT value in the PHOTOS version with multiphoton emission is equal to 10^{-7} of a typical energy scale[2] by default. The COMPASS spectrometer is not able to detect photons of energy below approximately 1 GeV. This corresponds to the energy resolution of the future electromagnetic calorimeter. Therefore we introduce a 1 GeV cut on the energy of the emitted photons to obtain results valid from the experimental point of view. Studies were performed to understand how much the hard photon emission depends on the XPHCUT value using the 1 GeV cut on the photons energy. The results are shown in Table 4.1.

As expected, both the global number of the detected photons and the number of the photons detected within the individual hadron decays, do not change significantly with the XPHCUT value while the number of the soft photons is very sensitive to it. This fact does not change any PHOTOS results. The soft photon emission is treated as if it would not exist and the events with soft photons enter the class of the events without photon emission. Conclusion of these studies is that hard photon emission does not depend on the XPHCUT value. Its default value of 10^{-7} did not need to be modified.

[2]If the incoming muon beam energy, 160 GeV, is chosen as a scale, the XPHCUT value may be given a value 10 keV.

XPHCUT	10^{-7}	10^{-6}	10^{-5}	10^{-4}
Photons generated in all decays				
number of photons with $E_\gamma > 1$GeV	**2333**	**2384**	**2229**	**2300**
number of photons with $E_\gamma \leq 1$GeV	160724	134836	108052	82963
Photons in decays of respective hadrons				
ρ^0 decay: number of photons with $E_\gamma > 1$GeV	**1149**	**1174**	**1078**	**1108**
ρ^0 decay: number of photons with $E_\gamma \leq 1$GeV	56107	47766	39132	30692
ω decay: number of photons with $E_\gamma > 1$GeV	**221**	**218**	**228**	**228**
ω decay: number of photons with $E_\gamma \leq 1$GeV	27655	23132	18275	13990
K_S^0 decay: number of photons with $E_\gamma > 1$GeV	**128**	**125**	**126**	**108**
K_S^0 decay: number of photons with $E_\gamma \leq 1$GeV	9914	8243	6569	5010
K^* decay: number of photons with $E_\gamma > 1$GeV	**151**	**144**	**127**	**137**
K^* decay: number of photons with $E_\gamma \leq 1$GeV	11342	9422	7567	15724

Table 4.1: Number of generated photons dependence on the XPHCUT parameter value.

4.4 Algorithm for Finding *Bremsstrahlung* Photons

When working with a Monte Carlo event, PHOTOS does not introduce to it any fundamental changes but adds in different places information on generated photons. A flowchart in Fig. 4.5 presents an algorithm constructed to find all the detectable *bremsstrahlung* photons in the event output.

Before calling PHOTOS a copy of the generated event record is made and two additional pieces of information are saved: the number of children of particles with a "decaying particle" status and the total number of particles for each generated event. After calling PHOTOS events with changed number of particles, probably due to adding new photons, are analysed. In a loop over all the particles photons and their mothers are found and the number of children of the photon mother is counted. In the next step the pointer of the photon mother in the copy of the event is found. The photon emission changes the order in the output; therefore in the case of the emission of several photons in one event it is very probable that the current pointer to the mother differs from the pointer to the same mother before PHOTOS. After taking that fact into account, events with different number of children before and after PHOTOS are analysed. In a loop over children which are photons and were not present before calling PHOTOS, a photon of largest energy is selected. If this

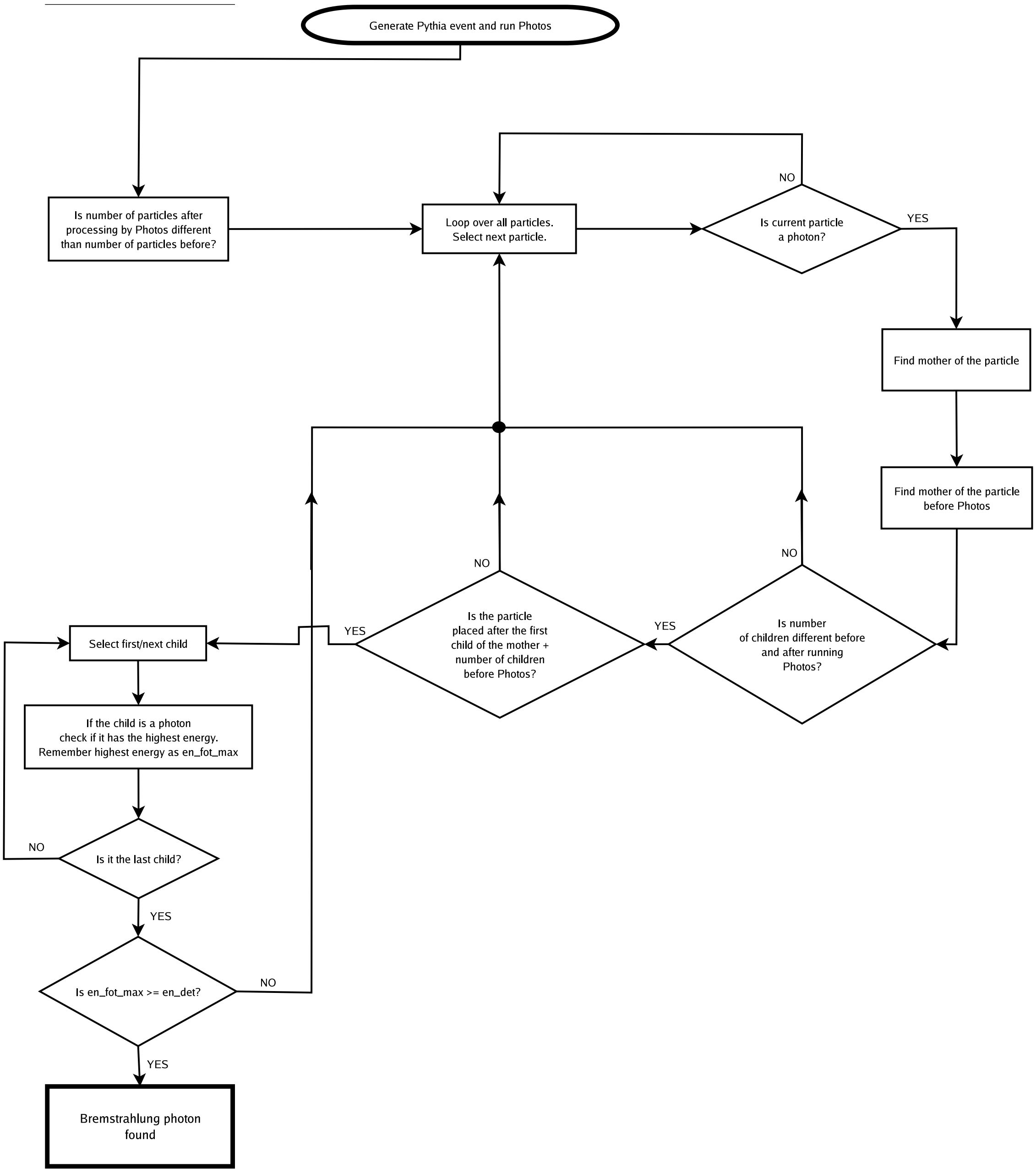

Figure 4.5: Flowchart of the *bremsstrahlung* photons finding algorithm used in this analysis.

photon has enough energy to be detected by a spectrometer, e.g. $E_\gamma \geq 1$ GeV, it is counted as a *bremsstrahlung* photon. In case of the multiphoton emission it was checked that if one of the photons fulfilled the detection condition, the remaining photons had energies $E_\gamma < 1$ GeV. Therefore all decays with multiphoton final state and those with one hard photon are jointly classified as decays with one photon. If none of the photons fulfilled the detection condition, *i.e.* all the photons are too soft, the event is classified as one without any photon emission. In the next step the correctly classified events with photon emission are transformed to the reference frame of the decaying particle where further analysis is performed.

The following checks were performed to ensure a correctness of the algorithm:

- change in the number of entries after PHOTOS was caused exclusively by generated photons
- pointers to the *bremsstrahlung* photons and to their "mothers" before and after PHOTOS were correct found
- all the generated photons were properly classificated with respect to their energy.

Chapter 5

Results of PHOTOS

In this Chapter results of PHOTOS are described; these comprise probability of the photon emission and properties of the emitted photons in the laboratory system and in the rest frame of the decaying particle. Next, distributions of different quantities crucial for ΔG analysis and possibly affected by photon emission such as the pion momenta, p_T of hadrons and the invariant mass of ρ^0 are shown.

5.1 Origin of Photons and Probability of the Photon Emission

A total sample of $50 \cdot 10^6$ events of $\mu^+ p$ scattering were generated. Among them 117463 *bremsstrahlung* photons with $E_\gamma \geq 1$ GeV were found[1]. Emitted photons come from decays of hadrons, e.g. ρ, ω, K^*, K^0_S mesons, cf. Table 5.1.

Nearly half of the *bremsstrahlung* photons originate at the ρ^0 decays. The ρ^0 meson in approximately 100% decays strongly into charged pions, $\rho^0 \to \pi^+\pi^-$ [3]. From now on only photons emitted at the ρ^0 decays in the above channel will be analysed. The probability of the photon emission is found to be very small, about a few permilles, see Table 5.2.

[1] In what follows by *bremsstrahlung* photons we shall mean those photons emitted in the hadron decays which fulfil the condition: $E_\gamma \geq 1$ GeV in the LAB system.

origin of photons	percent of emitted photons
ρ^0	47.3
$\rho^\pm$	29.2
ω^0	9.4
$K^{*0}, K^{*\pm}$	6.1
K^0_S	5.1
$D^0, D^\pm, D^{*\pm}$	1.6
η	0.6
Δ	0.5
ϕ, Σ, Λ	~ 0.1

Table 5.1: Origin of *bremsstrahlung* photons.

normalised to:	probability of *bremsstrahlung* emission
number of generated events	0.23%
number of all the possibilities	0.09%
number of $\pi^\pm$ from ρ^0 decays	0.14%

Table 5.2: Probability of the photon emission generated by PHOTOS. The expression "possibilities" in the second row means all decay branches in the generated event sample with at least one charged decay product.

5.2 Momentum Distribution of Emitted Photons in LAB

Momenta of the emitted photons have very wide spectra. Most of them are softer than charged hadrons, e.g. pions, which are the best candidates to be photon "mothers": an average momentum carried out by the emitted photons is 2.5 GeV, whereas the average momentum of pions is 3.4 GeV (cf. Figures 5.1 and 5.2). We remind the reader that the analysis presented here is limited to charged pions originating from the ρ^0 decays, see

Sec. 3.3. In particular average momenta of photons at the ρ^0 decays, about 2.6 GeV, are a little larger than average momenta of all the emitted photons; Fig. 5.3.

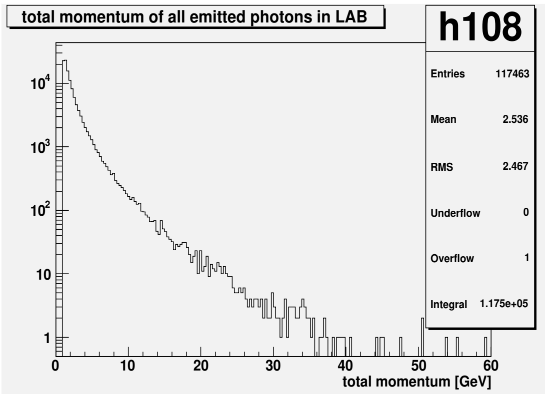

Figure 5.1: Momentum distribution of *bremsstrahlung* photons in LAB.

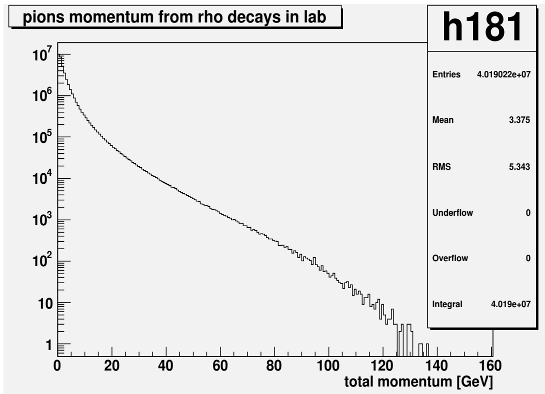

Figure 5.2: Momentum distribution of pions from ρ^0 decays in LAB.

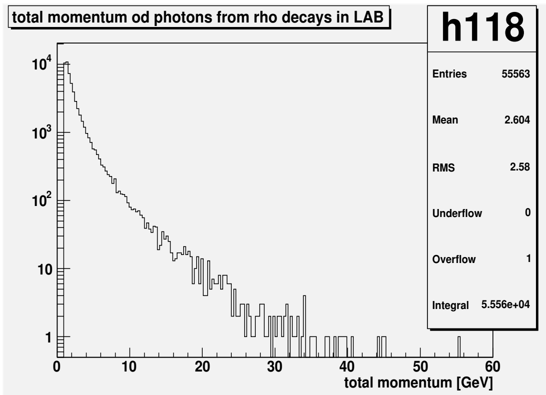

Figure 5.3: Momentum distribution of *bremsstrahlung* photons at the ρ^0 decays in LAB.

5.3 Properties of Emitted Photons in the Rest Frame of the Decaying Particle

5.3.1 Momentum distribution

Properties of the emitted photons are considered in the rest frame of a decaying particle, *i.e.* the rest frame of the ρ^0. Its mass and width are equal to 768.5 MeV and 151 MeV, respectively. The coordinate system we define in such a way that the momentum of the π^+ meson is along $+Z$ axis. In the absence of photons the momentum of π^- is along $-Z$ and the pions' average momentum due to non-zero width of the ρ^0 resonance is 0.358 GeV. Emission of *bremsstrahlung* photons causes an additional smearing of the pion momenta. Energy distribution of the emitted photons is shown in Fig. 5.4. The average energy is about 0.1 GeV. Photons carry approximately 40% of the pions' energy (cf. Fig. 5.5).

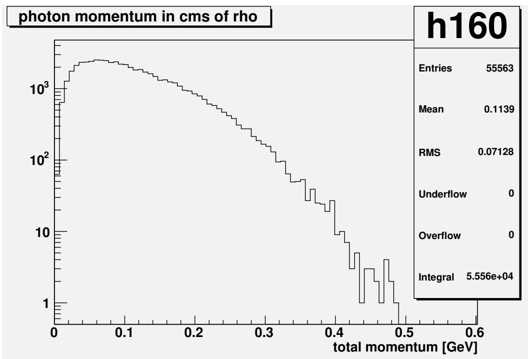

Figure 5.4: Energy of emitted photons in the ρ^0 rest frame.

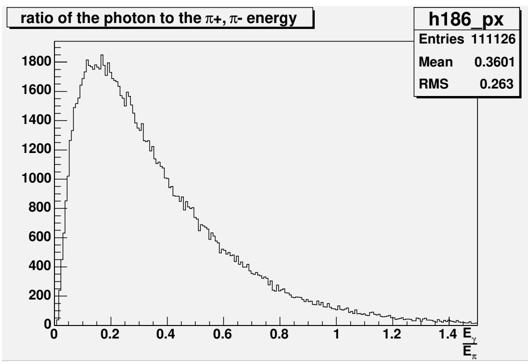

Figure 5.5: Ratio of the photon energy to the pion energy in the ρ^0 rest frame. There are two entries for each decay.

5.3.2 Angular distributions

PHOTOS gives information in which hadron decay a photon was created but it does not say which of decay products actually radiated. Due to this difficulty a photon emission angle cannot be defined. However, focusing on the ρ^0 decays into two charged pions, we can analyse distributions of α, the angle between an emitted photon and a decay pion, see Fig. 5.6.

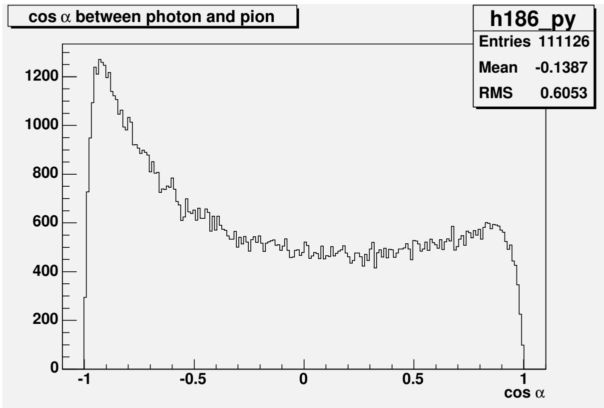

Figure 5.6: Cosine of the angle between a photon and a pion in the rest frame of ρ^0. There are two entries for each decay.

There is a maximum at $\cos\alpha = -1$ which means that most of the photons are emitted close to one of the pions. Approximately flat distribution outside the maximum means that the remaining photons are emitted isotropically.

5.3.3 "Wrong" events

Certain regions of the kinematically allowed phase space may not be properly described by PHOTOS [15]. Suspected are photons which fulfil two conditions: large angles α_i between a photon and a decay product i and also significant amount of energy carried out by the photon as compared to the remaining decay products energy [17]. The worst situation is a symmetric case when the angle between each pair of decay products, including photon, is about 120° ($\simeq$ 2.1 rad). Figures 5.7 and 5.8 illustrate how often the emission of hard photon with large angles takes place. The number of "wrong" photons dependence on the chosen kinematic cuts is summarized in Table 5.3. Number of photons from the "suspected" parts of the phase space is of the order of a few percent of all the emitted and detected photons.

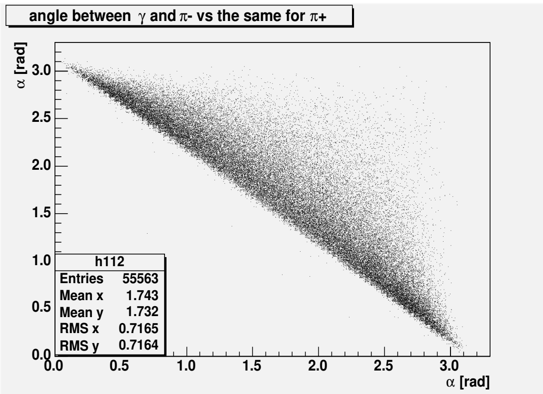

Figure 5.7: Angle between a photon and a π^- *vs* angle between a photon and a π^+.

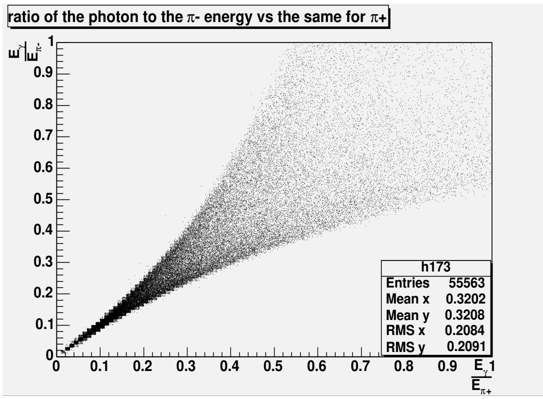

Figure 5.8: Ratio of the photon and π^- energies *vs* ratio of the photon and π^+ energies.

cuts		number of "wrong" photons	% of "wrong" photons
$\alpha[rad]$	$E_\gamma/E_{\pi^\pm}$		
> 1.57	> 0.5	4479	3.8
	> 0.6	4185	3.6
	> 0.7	2943	2.5
	> 0.8	1861	1.6
> 1.74	> 0.5	3630	3.1
	> 0.6	3026	2.6
	> 0.7	2353	2.0
	> 0.8	1669	1.4
> 1.92	> 0.5	1713	1.5
	> 0.6	1703	1.4
	> 0.7	1594	1.3
	> 0.8	1312	1.1

Table 5.3: Number of "wrong" photons for different kinematic cuts.

5.4 Momentum Distributions of Pions from the ρ^0 Decays

Charged pions are the particles most frequently produced in the final state of the $\mu^+ p$ interaction. They are also the most radiating ones. Therefore it was checked how much does the *bremsstrahlung* emission change their LAB momenta distributions. From the whole sample of pions coming from the ρ^0 decays a subset containing pions which have subsequently emitted photons was selected. Further analysis was performed on these subsamples parallely. All the distributions were done using PYTHIA and they are shown in two stages: before being affected by PHOTOS (later called in short "before PHOTOS") and after being affected by PHOTOS ("after PHOTOS"). The effects of the photon emission by pions checked on a very high number of generated events were found to be very small, therefore all the distributions and their ratios are presented without errors.

Momenta of pions which have emitted photons and their transverse momenta with respect to the γ^* momentum are observables most affected by the *bremsstrahlung* emission. They are presented in Figures 5.9 – 5.16. Distributions of the same quantities but for the whole sample of the pions from the ρ^0 decays are shown in Figures 5.17 – 5.24.

As expected the pions momenta and their transverse momenta distributions in a subsample with *bremsstrahlung* become narrower due to the photon radiation (see Figures 5.9 and 5.13). After applying PHOTOS there is more soft and less hard pions than before (cf. Figures 5.12 and 5.15). The pions average momenta and transverse momenta after PHOTOS change compared to those before: 9.3 GeV *vs* 8.0 GeV and 0.37 GeV *vs* 0.31 GeV respectively. The changes are large and reach up 50% as in Fig. 5.16. The observed differences in a subsample of pions which have subsequently emitted photons have a meaning of an upper limit of the effect since experimentally we are not able to separate radiating and non radiating pions. The changes in the distribution of the momenta and of the tansverse momenta of all the $\pi^\pm$ resulting from the ρ^0 decays look similar but are smaller than a fraction of a percent (see Figures 5.20 and 5.24). The average momenta and the transverse momenta after PHOTOS change insignificantly from 3.38 GeV to 3.37 GeV and from 0.344 GeV to 0.343 GeV respectively.

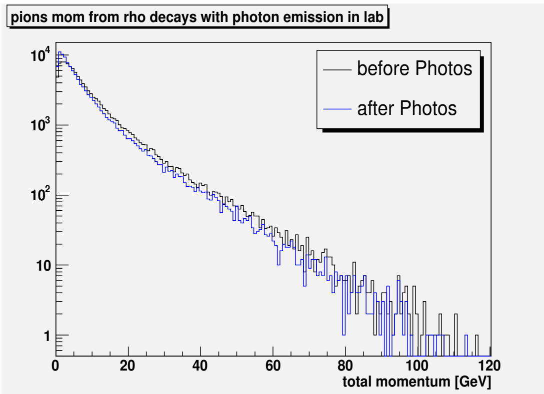

Figure 5.9: The $\pi^{\pm}$ momentum distributions in the laboratory before and after applying PHOTOS. Only pions which have subsequently emitted photons enter the distributions.

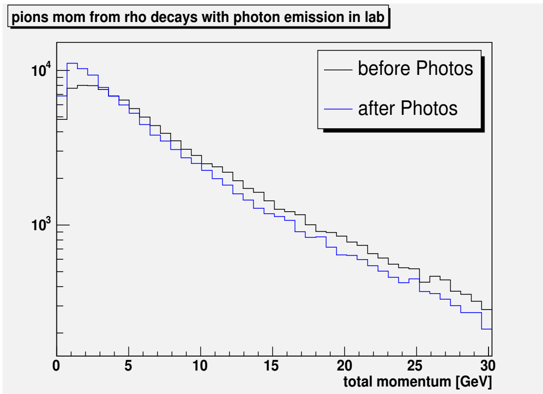

Figure 5.10: Same as in Fig. 5.9 in the range $0 - 30$ GeV.

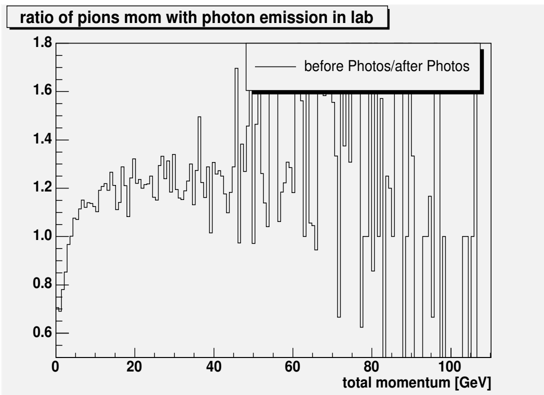

Figure 5.11: Ratio of the $\pi^{\pm}$ momentum distributions in the laboratory before and after applying PHOTOS. Only pions which have subsequently emitted photons enter the distributions.

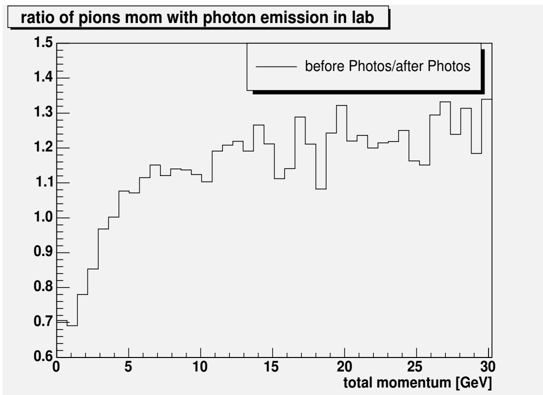

Figure 5.12: Same as in Fig. 5.11 in the range $0 - 30$ GeV.

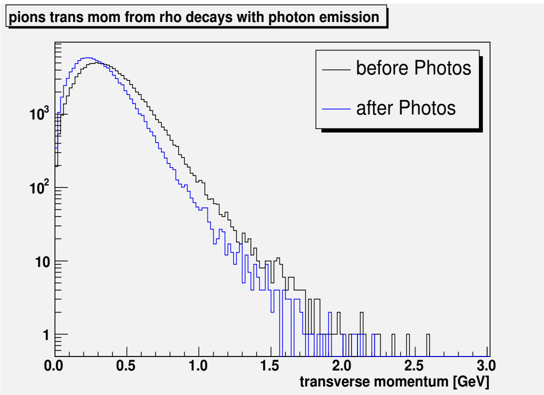

Figure 5.13: The $\pi^{\pm}$ transverse momentum distributions in the laboratory before and after applying PHOTOS. Only pions which have subsequently emitted photons enter the distributions.

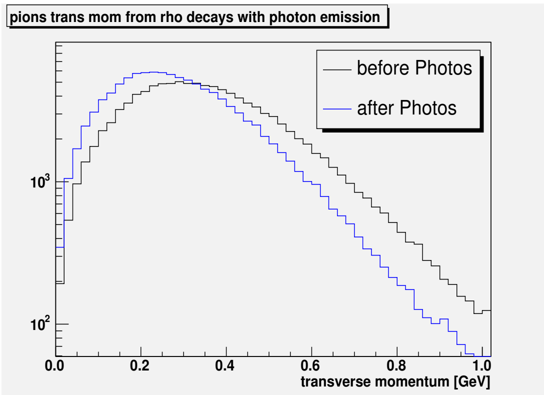

Figure 5.14: Same as in Fig. 5.13 in the range $0 - 1$ GeV.

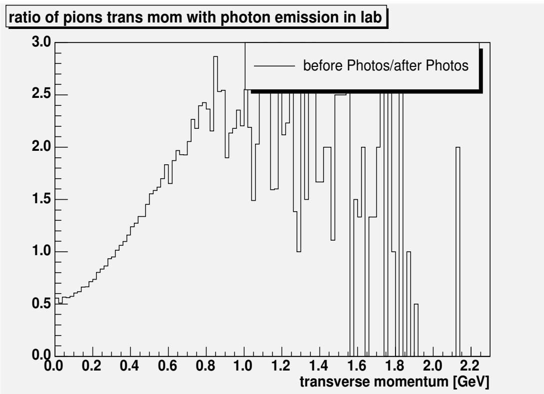

Figure 5.15: Ratio of the $\pi^{\pm}$ transverse momentum distributions in the laboratory before and after applying PHOTOS. Only pions which have subsequently emitted photons enter the distributions.

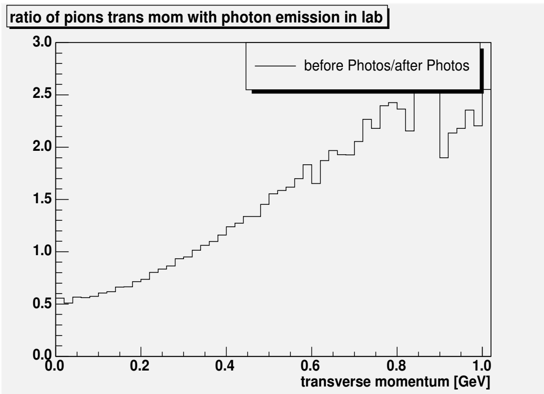

Figure 5.16: Same as in Fig. 5.15 in the range $0 - 1$ GeV.

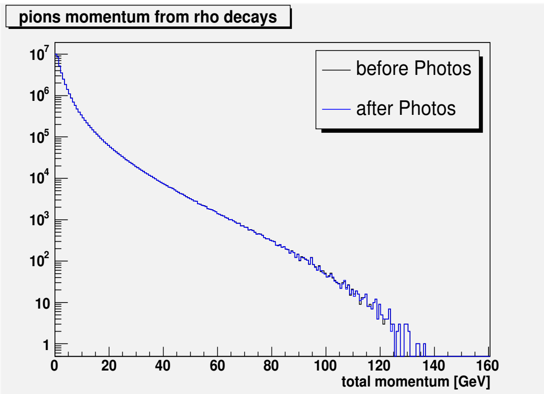

Figure 5.17: The $\pi^{\pm}$ momentum distributions in the laboratory before and after applying PHOTOS. All pions originating from the ρ^0 decays enter the distributions.

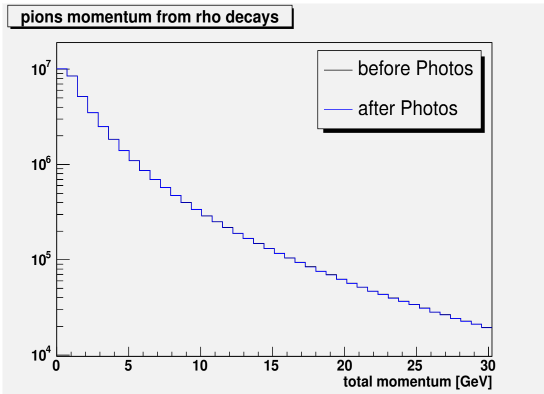

Figure 5.18: Same as in Fig. 5.17 in the range $0 - 30$ GeV.

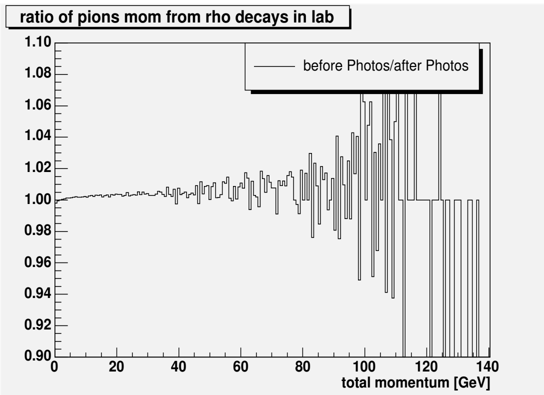

Figure 5.19: Ratio of the $\pi^{\pm}$ momentum distributions in the laboratory before and after applying PHOTOS. All pions originating from the ρ^0 decays enter the distributions.

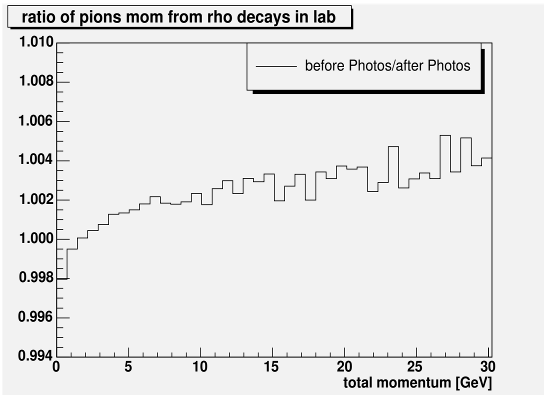

Figure 5.20: Same as in Fig. 5.19 in the range $0 - 30$ GeV.

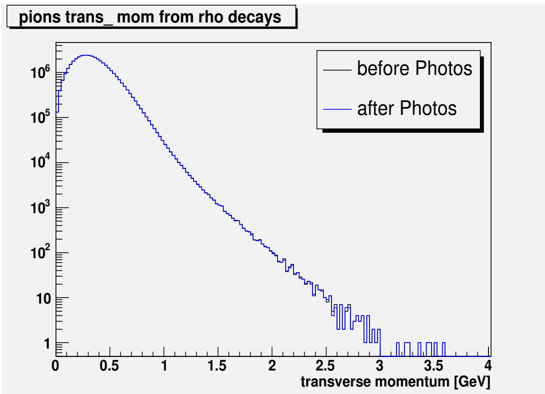

Figure 5.21: The $\pi^{\pm}$ transverse momentum distributions in the laboratory before and after applying PHOTOS. All pions originating from the ρ^0 decays enter the distributions.

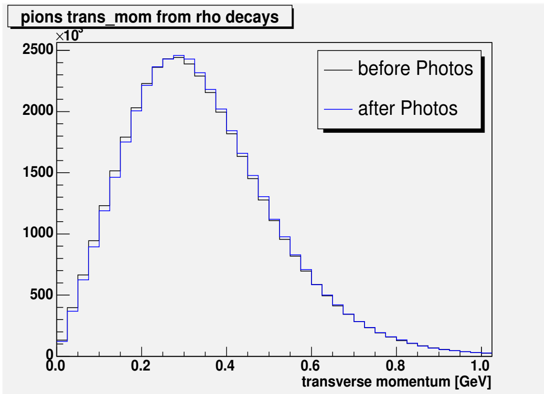

Figure 5.22: Same as in Fig. 5.21 in the range $0 - 1$ GeV

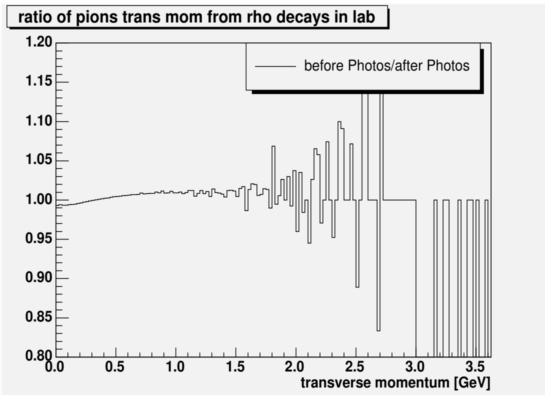

Figure 5.23: Ratio of the $\pi^{\pm}$ transverse momentum distribution in the laboratory before and after applying PHOTOS. All pions originating from the ρ^0 decays enter the distributions.

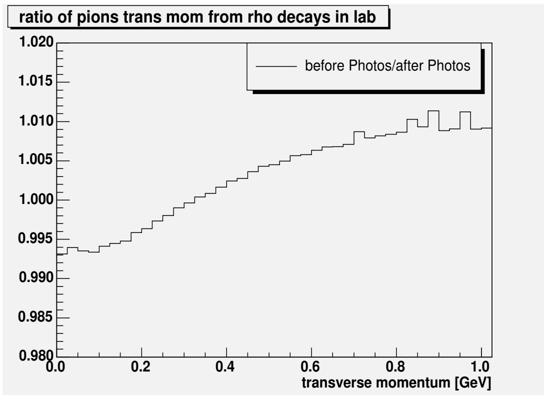

Figure 5.24: Same as in Fig. 5.23 in the range $0 - 1$ GeV.

5.5 Distribution of High p_T Hadron Pairs

The cuts selecting high p_T hadron pairs in the COMPASS data, used in the analysis of ΔG [4], are the following:

$$p_{T_1} > 0.7\,\mathrm{GeV}, \quad p_{T_2} > 0.7\,\mathrm{GeV}, \quad p_{T_1}^2 + p_{T_2}^2 > 2.5\,\mathrm{GeV}^2 \tag{5.1}$$

Therefore the same cuts are applied to define high p_T hadron pairs in this analysis. For each generated event a hadron pair, consisting of a hadron with the highest p_T and a hadron with the next highest p_T, is selected. If hadrons fulfil the condition 5.1 they enter the further analysis. The transverse momentum distribution of the hadron with the highest p_T, later called "1st hadron", before applying PHOTOS is shown in Fig. 5.25. The same for the next-to-the highest p_T hadron,"2nd hadron", is presented in Fig. 5.27[2]. In Figures 5.26 and 5.28 are shown ratios of the transverse momenta before and after PHOTOS for the 1st and the 2nd hadron, respectively.

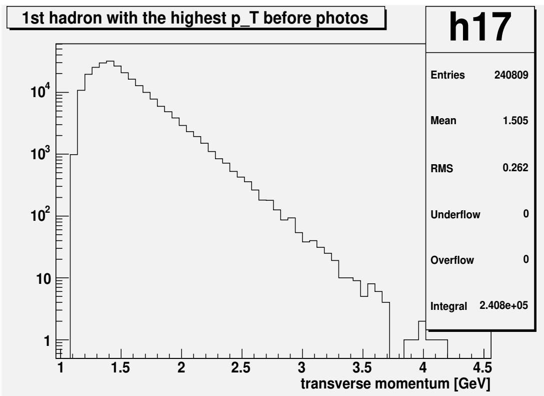

Figure 5.25: The 1st hadron p_T distribution before applying PHOTOS.

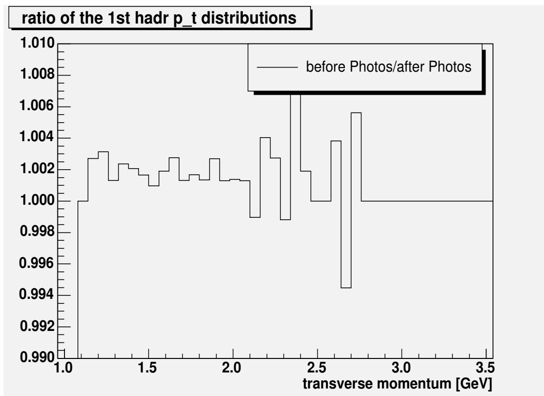

Figure 5.26: Ratio of the 1st hadron p_T distributions before and after applying PHOTOS.

Bremsstrahlung radiation causes that about 0.2% less events fulfil the conditions 5.1 both in the sample of the 1st hadron and of the 2nd hadron, Figures 5.26 and 5.28. It was checked that all the missing events after PHOTOS were the events with photon emission. The observed behaviour is self-explanatory – photons emitted out momentum, therefore there should be less particles with high transverse momenta.

[2]The flat top of the distribution in the range $0.8 - 1.1$ GeV is observed also in the real data [4] and is due to kinematic cuts.

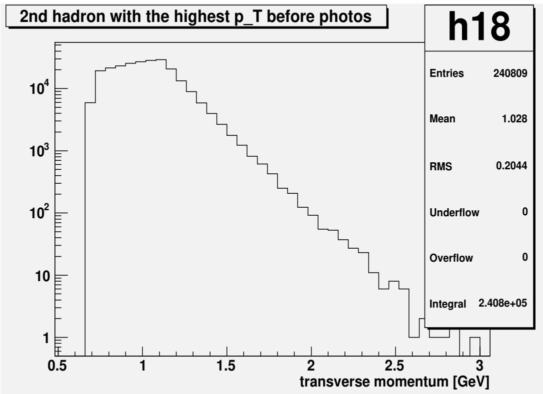

Figure 5.27: The 2nd hadron p_T distribution before applying PHOTOS.

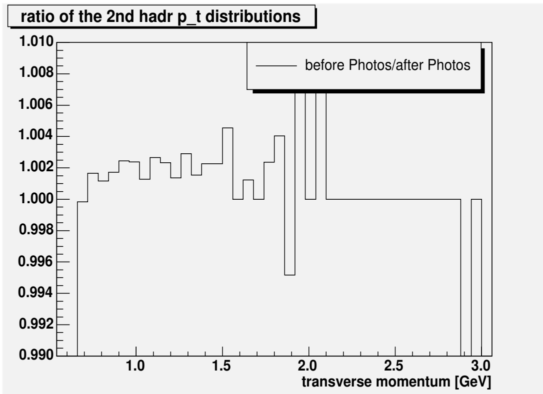

Figure 5.28: Ratio of the 2nd hadron p_T distributions before and after applying PHOTOS.

5.6 Distribution of the Invariant Mass of ρ^0

One of the goals of the COMPASS analysis is investigating the exclusive[3] vector mesons (such as ρ^0) production. Thus it would be desirable to check how much the *bremsstrahlung* emission influences the distribution of the invariant mass of ρ^0. Here, because of much higher statistics available, the inclusively[4] produced ρ^0 was analysed instead. In Figures in this Section a difference between a $\pi^+\pi^-$ invariant mass and a nominal mass of the ρ^0 meson, 768 MeV, is piloted.

The analysed ρ^0 decay channel: $\rho^0 \to \pi^+\pi^-$ has a branching ratio of nearly 100% [3]. It is expected that the mass distribution of the $\pi^+\pi^-$ pairs from ρ^0 decays would be described by the Breit-Wigner curve centred on 768.5 MeV with the full-width at half maximum about 151 MeV. However, the mass distribution obtained from the PYTHIA generator is shifted towards lower values (is centred on 750 MeV), has smaller full-width (about 125 MeV) and its shape is non symmetrical, see Fig. 5.29. All these features are inherent for PYTHIA [19]. In Figures 5.30– 5.32 the $\pi^+\pi^-$ pairs mass distributions before and after applying PHOTOS for those ρ^0 decays at which photon emission took place are presented.

Bremsstrahlung emission simulated by PHOTOS changes significantly the $\pi^+\pi^-$ invariant mass distribution. Before PHOTOS it is centred on 790 MeV and after PHOTOS – on 660 MeV, see Figures 5.30 and 5.31. These changes indicate that the photons carry out the energy and momentum from the ρ^0 centre-of-mass and thus after PHOTOS a large excess

[3]Exclusive production means that the only particle produced is ρ^0: $\mu\, N \to \mu\, N\, \rho^0$.

[4]Inclusive production means that the only hadron identified in the final state is ρ^0: $\mu\, N \to \mu\, \rho^0\, X$.

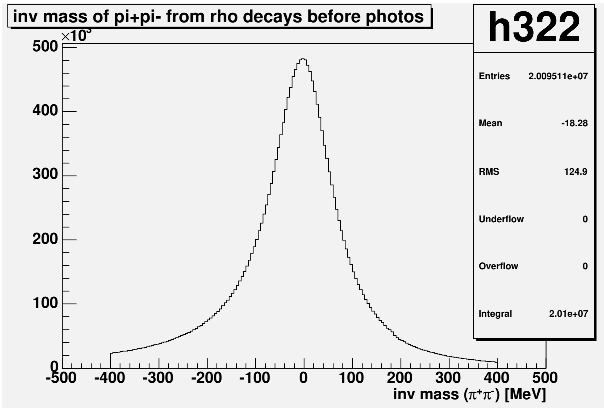

Figure 5.29: Invariant mass distribution of all the π^+ π^- pairs from ρ^0 decays generated by PYTHIA.

of low energy $\pi^+\pi^-$ pairs is observed.

Those $\pi^+\pi^-$ pairs which have subsequently emitted a photon are not a random subset of all the $\pi^+\pi^-$ pairs because distributions of the ρ^0 invariant mass in those two subset are different, cf. Figures 5.29 and 5.30. Distribution in Fig. 5.30 is shifted towards higher values of the ρ^0 invariant mass and has inverse asymmetry in the "tails". These differences are obvious if we recall that the probability of the photon emission is directly proportional to the kinematically allowed energy in the centre-of-mass of a decaying particle. Photons emission at the high energy ρ^0 decays is more probable than at the lower energy ρ^0 decays, hence the observed shift in the $\pi^+\pi^-$ mass distribution in Figures. 5.29 and 5.30.

In Figures 5.33 and 5.34 the invariant $\pi^+\pi^-$ pairs mass distributions of all the inclusive ρ^0 before and after applying PHOTOS, respectively, are shown. The changes in both distributions are similar to those for the subset of ρ^0 which have subsequently emitted photons albeit much less significant, cf. Fig. 5.36. After PHOTOS there is less high energy $\pi^+\pi^-$ pairs and more low energy ones. The effect is of the order of 2%.

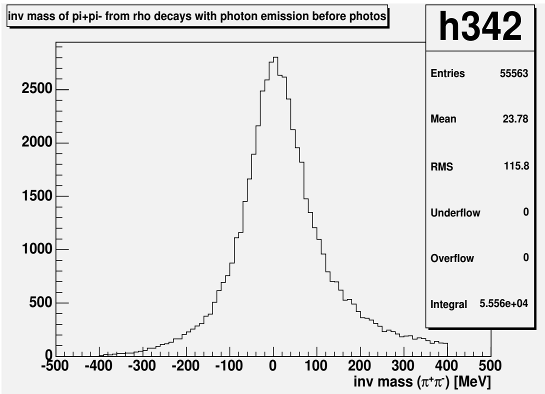

Figure 5.30: Invariant mass of $\pi^+\pi^-$ pairs coming from those ρ^0 decays which have subsequently emitted photons.

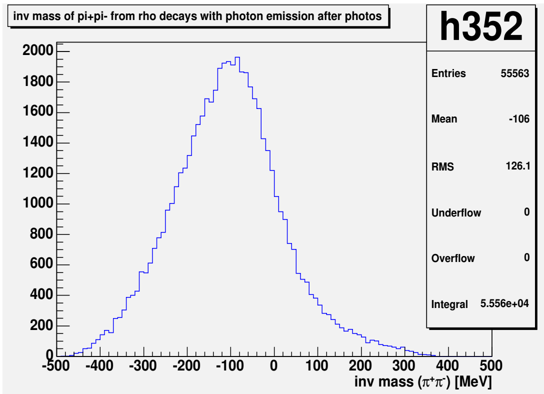

Figure 5.31: Same as in Fig. 5.30 but after applying PHOTOS.

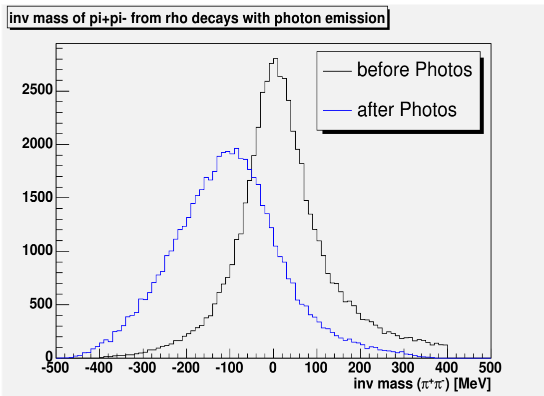

Figure 5.32: Comparison of the distributions 5.30 and 5.31.

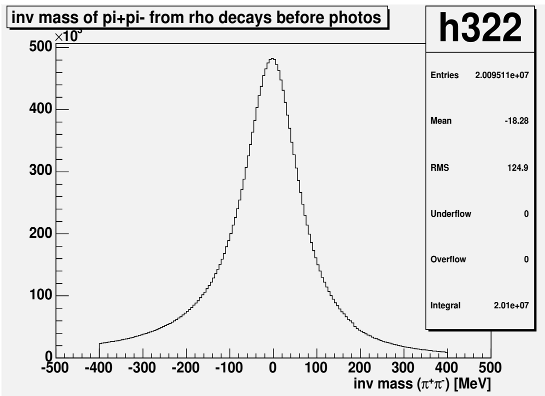

Figure 5.33: Invariant mass of $\pi^+\pi^-$ pairs coming from all the ρ^0 decays.

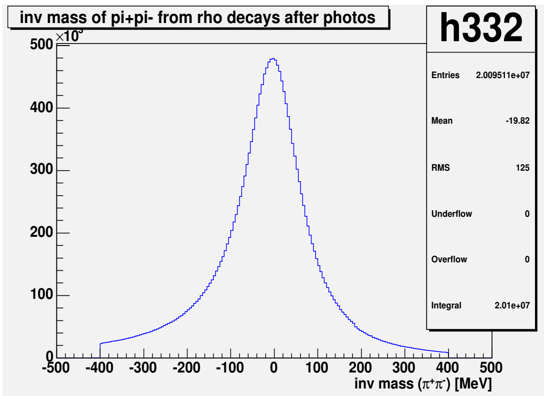

Figure 5.34: Same as in Fig.5.33 but after applying PHOTOS.

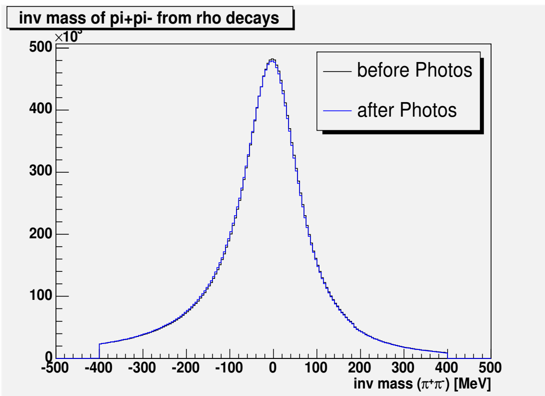

Figure 5.35: Comparison of the distributions 5.33 and 5.34.

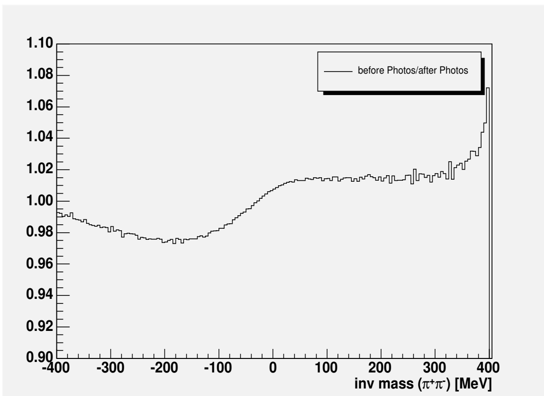

Figure 5.36: Ratio of the distributions 5.33 and 5.34.

Chapter 6

Conclusions

Since the late eighties when the EMC experiment published its results on a negligible quark contribution to the nucleon spin, the spin puzzle of the nucleon remains unsolved. The COMPASS experiment at CERN with the rich spin physics programme is one of the presently running experiments whose goal is a direct measurement of the gluon polarisation in the nucleon. This aim will be achieved in two independent ways: by detection of open charm mesons and of high p_T hadron pairs in the final state. Both analyses require a correct identification of hadrons and a correct measurements of their four-momenta. All potential systematic biases of those observables like radiative corrections should be carefully studied.

This thesis is a first attempt to simulate QED radiative corrections in the decays of hadrons in COMPASS. All the presented simulations were done by the PYTHIA generator combined with PHOTOS, a dedicated Monte Carlo generating photons in decays of particles. A total sample of $50 \cdot 10^6$ events were generated, among them 117463 of *bremsstrahlung* photons were found. PHOTOS usage in COMPASS is justified because about 70% of charged pions and 50% of charged kaons come from decays of other particles. Probability of emitting photons detectable by the spectrometer was found to be very small. Only about 0.14% of charged pions from the ρ^0 decays emit photons.

Results presented in this work we can summarize as follows:

- differences between the distributions of both the momentum and the transverse momentum of pions before and after applying PHOTOS are of the order of a few permilles;
- shape of the high p_T hadron pairs distribution does not change after applying PHOTOS;
- change in the number of the high p_T hadron pairs after applying PHOTOS is of the order of a few permilles;

- the largest difference before and after applying PHOTOS is observed between distributions of in the $\pi^+\pi^-$ invariant mass; it is of the order of a few percent.

We conclude that adding *bremsstrahlung* photon emission modelled by the PHOTOS Monte Carlo program [13] to the hadron vertex of the inelastic $\mu^+ N$ scattering does not have any significant effect on the distributions of the quantities used in the COMPASS data analysis. Results obtained in this thesis confirm a popular conviction that the QED radiative corrections to the hadron current are negligible.

Podziękowania

Serdecznie dziękuję tym, którzy swoim wsparciem, radą i cierpliwym towarzyszeniem przyczynili się do powstania tej pracy. W sposób szczególny dziękuję Pani prof. B. Badełek, Panu dr hab. Z. Wąsowi, G. Bronie i M. Stolarskiemu. Dziękuję pozostałym członkom warszawskiej grupy COMPASS za cenne uwagi i dyskusje.

Bibliography

[1] EMC, J. Ashman *et al.*, Phys. Lett. **B 206**, 364 (1988); Nucl. Phys. **B 328**, 1 (1989).

[2] SMC, D. Adams *et al.*, Phys. Rev. **D 58**, 112002 (1998).

[3] S. Eidelman *et al.*, Phys. Lett. **B 592**, 1 (2004).

[4] Preliminary results on ΔG from high p_T hadron pairs at $Q^2 < 1\,\mathrm{GeV}^2$ are given in: C. Bernet (COMPASS), talk presented at The 13th International Workshop on Deep Inelastic Scattering, DIS05, *http://www.hep.wisc.edu/dis05/*;
C.Bernet, S. Hedicke, J.M. Le Goff, S. Procureur (COMPASS), *Measurement of $\Delta G/G$ in the production of high p_T hadron pairs at low Q2 (2003 data)*, COMPASS note, 2005-9.

[5] L.W.Mo, Y.S. Tsai, Rev. Mod. Phys. **41**, 205 (1969); Y.S.Tsai, SLAC-PUB-848, (1971).

[6] A.A. Akhundov, D. Bardin, L. Kalinovskaya, T. Riemann, Fortschr. Phys. **44**, 373 (1996).

[7] B. Badełek, D. Bardin, K. Kurek, C. Scholtz, Z. Phys. **C 66**, 591 (1995).

[8] T. Sjöstrand *et al.*, Comp. Phys. Comm. **135**, 238 (2001).

[9] G. Ingelman, J. Rathsman, G. A. Schuler, Comp. Phys. Comm. **101**, 135 (1997).

[10] G. Ingelman, A. Edin, J. Rathsman, *LEPTO 6.5 – A Monte Carlo Generator for Deep Inelastic Lepton-Nucleon Scattering*, DESY 96-057.

[11] I. Akushevich, H. Böttcher, D. Ryckbosch, RADGEN 1.0 *Monte Carlo Generator for Radiative Events in DIS on Polarized and Unpolarized Targets*, hep-ph/9906408.

[12] P. Liebing, Ph. D. thesis *Can the Gluon Polarization in the Nucleon be extracted from HERMES Data on single high-pt Hadrons?*, Universitaet Hamburg, 2004, *http://www-hermes.desy.de/*.

[13] E. Barberio, Z. Wąs, Comp. Phys. Comm. **79**, 291 (1994).

[14] Z. Wąs, *http://wasm.home.cern.ch/wasm/goodies.html*.

[15] Z. Wąs, P. Golonka, *PHOTOS Monte Carlo: a precision tool for QED corrections in Z and W decays*, IFJPAN-V-05-01, CERN-PH-TH/2005-091.

[16] B. Kersevan (ATLAS), *http://borut.home.cern.ch/borut/*.

[17] Z. Wąs, *private communication*, October 2004 – June 2005.

[18] B. Kersevan (ATLAS), *private communication*, November 2004.

[19] T. Sjöstrand, *private communication*, May 2003.